http://dx.doi.org/10.5935/0103-5053.20140271

J. Braz. Chem. Soc., Vol. 25, No. 12, 2444-2454, 2014.
Printed in Brazil - ©2014 Sociedade Brasileira de Química
0103 - 5053 $6.00+0.00

Article

Influence of Temperature and Time of Seed Aging on the Properties of Beta Zeolite/MCM-41 Materials

Saulo T. F. Grecco,[a] Ernesto A. Urquieta-González,[b] Patrício Reyes,[c] Marcelo Oportus[c] and Maria do Carmo Rangel[*,a]*

[a]*Grupo de Estudo em Cinética e Catálise (GECCAT), Instituto de Química, Universidade Federal da Bahia, Campus Universitário de Ondina, Federação, 40170-290 Salvador-BA, Brazil*

[b]*Departamento de Engenharia Química, Universidade Federal de São Carlos, 13565-905 São Carlos-SP, Brazil*

[c]*Facultad de Ciências Químicas, Universidad de Concepción, Casilla 3-C, Concepción, Chile*

As restrições de difusão dos reagentes, causadas pelos microporos, limitam a utilização de zeólitas no processamento de moléculas volumosas. Isto exige o desenvolvimento de materiais que combinem as propriedades das zeólitas com aquelas dos materiais mesoporosos. Com este objetivo, neste trabalho, estudou-se a influência da temperatura e do tempo de envelhecimento de sementes nas propriedades de materiais do tipo zeólita beta/MCM-41, obtidos por mesoestruturação/cristalização. Observou-se que as condições adequadas para obter a fase cristalina microporosa de zeólita beta e a fase mesoporosa MCM-41 foi 140 °C, durante 24 h de envelhecimento das sementes. Nas demais temperaturas (60 e 90 °C) foram produzidos sólidos menos cristalinos e uma fase lamelar de MCM-50. Por outro lado, com o aumento do tempo de envelhecimento das sementes, foram obtidos cristais maiores da zeólita beta cristalina e fases mesoporosas menos organizadas a 140 °C.

The diffusion restrictions of the reactants caused by the micropores limit the use of zeolites for processing heavy molecules. This demands the development of materials that combine the properties of zeolites and mesoporous materials. With this goal in mind, the influence of temperature and time of seed aging on the properties of beta zeolite/MCM-41 materials obtained by mesostructuration/crystallization was studied in this work. It was noted that the most suitable conditions to obtain the crystalline microporous phase of beta zeolite and the MCM-41 mesoporous phase was 140 °C, during 24 h of seed aging. At the other temperatures (60 and 90 °C) poor crystallized solids and a lamellar phase of MCM-50 were produced. On the other hand, increasing time of aging seeds bigger crystals of crystalline beta zeolite and less organized mesoporous phases were obtained at 140 °C.

Keywords: beta zeolite, mesostructuration, MCM-41, seed aging, mesoporous ordering

Introduction

Many efforts have been devoted to the improvement of heterogeneous catalysts, aiming to obtain highly active and selective materials in the desired reactions. Among them, zeolites have become successful alternatives as catalysts for processes in the chemical and petrochemical industries.[1-5] These solids have high specific surface area, high adsorption capacity, pores with molecular dimensions and high thermal and hydrothermal stability.[6,7] However, zeolites show restrictions to the diffusion of bulky molecules because of their small micropores. The slow transport of reactants and products inside micropores leads to an increased residence time that favors undesirable reactions, such as coke production which causes the zeolite deactivation by the blockage of the channels. It is known[8] that the rate of coke formation and the coke composition as well as the catalyst deactivation depend on the pore structure and on the acidity of the zeolite, besides the operating conditions such as temperature, pressure and nature of the reactants.

In order to overcome the diffusion limitations, considerable efforts have been addressed for developing

*e-mail: mcarmov@ufba.br

zeolites containing mesopores with sizes similar to those of materials such as MCM-41, HMS and SBA-15.[9-11] These materials have ordered mesopores but exhibit lower acidity, as well as lower thermal and hydrothermal stability, as compared to zeolites and thus have limited application in catalysis.[12] Therefore, several strategies have been developed to prepare materials that can combine the advantages of zeolites and of mesoporous materials, especially the high acidity of the first one and the mesoporosity of the last one.[12-16] The most successful approaches involve the use of templates (organic agents or nanoparticles) for generating mesoporosity or nanocasting (confined-space synthesis) that produce solids with the intrinsic microporosity of zeolites besides an intrazeolitic mesoporosity with a narrow pore size distribution.[17]

The experimental observations have shown that the zeolitic precursors can be used as building blocks for a mesoporous network. The first methodology, developed by Pinnavaia and co-workers,[18] consisted in the organization of zeolitic precursors (FAU) in an ordered hexagonal mesophase of MCM-41-type. The supramolecular ordering of these precursors (also known as zeolite seeds) gives hydrothermal stability and acidity to the mesoporous structure. Several studies have been developed in order to obtain mesoporous materials assembled from zeolite seeds, such as Beta/MCM-41,[19-21] Beta/MCM-48,[22] ZSM-5/MCM-41[23] and mordenite/MCM-41 materials[24] Also, several materials were obtained from the assemblage of zeolitic precursors in a hexagonal mesoporous structure of SBA-15-type, such as Y/SBA-15, ZSM-5/SBA-15 and beta/SBA-15 materials.[25] However, for most cases, a mesoporous structure with crystalline walls was not obtained and a mixture of phases was observed. In spite of this fact, these materials have been often reported as zeolite/mesoporous phase composite. Guo *et al.*,[21] for instance, have described a solid named Beta/MCM-41 composite, although they have been observed, by scanning electron microscopy, that the crystals of beta zeolite were evenly incorporated into spherical aggregates of MCM-41.

Several studies have been performed in order to evaluate the influence of synthesis parameters, such as temperature and time of seed aging, crystallization temperature and gel composition on the properties of mesoporous materials assembled from beta zeolite seeds, although most of them have been unsuccessful, producing systems made up of two phases.[26-28] Some studies have shown that the time of hydrothermal treatment (aging time), during which the zeolite seeds are formed, is a key parameter to control the properties of the final material.[26-28] Also, in some cases, it was observed that the curvature of the surfactant micelle does not favor the assemblage of nanoparticles (zeolite seeds).[15] For example, the MCM-41-type materials have pore wall thickness in the order of 1 nm and then it would be very difficult to accommodate these nanoparticles (in the range from 20 to 150 nm for beta zeolite)[29] into a highly condensed crystalline wall. On the other hand, one can propose a cluster of silica/template, which leads to amorphous primary units in the range of 1-3 nm that fit better into the mesoporous wall. In order to obtain this silica/template cluster, lower aging temperature or shorter aging time must be used, which will favor the nucleation rate at the expense of growth rate. However, no crystalline zeolitic precursor of less than 5 nm has been detected by transmission electron microscopy (TEM) and no evidence of crystalline wall by TEM images or diffraction patterns have been reported so far.[15] On the other hand, higher temperatures lead to materials made of two phases, which show high performance in several reactions involving bulky reactants and products, making them promising catalysts for many processes of chemical and petrochemical industry.[30-34] In a previous work,[35] for instance, we have found that catalysts based on cobalt supported on beta zeolite/MCM-41 materials were very active and selective for Fischer-Tropsch synthesis.

Moreover, beta zeolite in the protonic form (H-BEA) has been reported as an excellent catalyst for several reactions catalyzed by acidic sites, especially for reactions of fine chemistry.[36,37] Examples of successful applications of beta zeolite include aromatic alkylation, aromatic acylation, indole synthesis, aromatic nitration and aliphatic alkylation.[37] Therefore, it is expected that new applications of these solids in catalysis can be found by combining the mesoporosity and the crystallinity of beta zeolite.

Aiming to improve the properties of assembled materials from beta zeolite seeds, the combined influence of temperature and time of seed aging on the properties of these solids was studied. Samples were obtained via mesostructuration with cetyltrimethylammonium bromide and subsequent hydrothermal crystallization. Several temperatures (60, 90 and 140 °C) were used for the seed aging for 24 h and then the seeds were crystallized at 140 °C, for 48 h. In a second step, different times (24, 48, 96 and 192 h) for the seed aging were used at 140 °C. These conditions have not been studied yet and are expected to produce more crystalline solids.

Experimental

Reagents and chemicals

Aerosil 200 fumed silica (Degussa, 100% purity), sodium aluminate (Riedel-de-Häen, 99.5% purity), sodium hydroxide (Merck, 99% purity), tetraethylammonium

hydroxide (TEAOH, Aldrich, 35% solution in water), cetyltrimethylammonium bromide (CTAB, Merck, 99% purity) and ammonium chloride (Merck, 99.8% purity) were used for sample preparation in this work.

Effect of aging temperature of the seed gel on the properties of beta zeolite/MCM-41 materials

For this study, the samples were prepared by mesostructuration/crystallization of beta zeolite seeds, using a method based on the methodology previously reported[4] but changing the conditions of seed aging and crystallization. The seed gel ($1.47Na_2O:Al_2O_3:29.5SiO_2:8.23TEAOH:368H_2O$) was obtained by mixing silica, sodium aluminate, sodium hydroxide, TEAOH and water. The gel obtained went on hydrothermal treatment at 60, 90 and 140 °C, for 24 h. Then the seed gel was mesostructured with CTAB by adjusting the pH between 9.0 and 9.5 and going on a hydrothermal treatment at 140 °C, for 48 h. After mesostructuration/crystallization, the samples were centrifuged, washed with deionized water and dried at 60 °C, for 24 h to obtain the as-synthesized materials in the sodium form (B60/24, B90/24 and B140/24 samples).

Effect of aging time of the seed gel on the properties of beta zeolite/MCM-41 materials

Based on the results of the experiments described, it was concluded that 140 °C was the most suitable aging temperature for obtaining the desired solid. This value has then been used for studying the effect of aging time on the properties of assembled materials from beta zeolite seeds. The samples were prepared by varying the time of gel aging (24, 48, 96 and 192 h) using the same procedure.

The solids were calcined at 550 °C, for 635 min to obtain the materials in the sodium form (B140/24, B140/48, B140/96 and B140/192 samples). Subsequently, ion exchange with ammonium chloride was performed at 65 °C, for 3 h, followed by filtration, washing and drying at 60 °C, for 24 h. The samples were then calcined at 550 °C for 635 min, to obtain the materials in the protonic form (HB140/24, HB140/48, HB140/96 and HB140/192 samples).

Sample characterization

The solids were characterized by X-ray diffraction, Fourier transform infrared spectroscopy, differential thermal analysis, thermogravimetry, nitrogen adsorption and desorption, acidity measurements by ammonia desorption and transmission electron microscopy.

The formation of the hexagonal mesoporous structure of MCM-41-type and of the microporous structure of beta zeolite in the samples was investigated by X-ray diffraction (XRD), performed in a Shimadzu XRD 6000 equipment, using CuKα radiation generated at 40 kV and 30 mA and a monochromator. The analysis was performed in the 2θ scanning range from 1 to 10° using a goniometer speed of 0.5° min^{-1} (for the mesoporous phase identification) and from 5 to 45° using a goniometer speed of 2.0° min^{-1} (for the microporous phase identification).

The removal of the template and the production of the zeolite structure were followed by Fourier transform infrared spectroscopy (FTIR). The experiments were performed in a Perkin Elmer Spectrum One spectrophotometer. For each spectrum, 32 scans were obtained in the range of 400 to 4000 cm^{-1} with a resolution of 4.0 cm^{-1}. The sample powder (about 50 mg) was mixed with 200 mg of potassium bromide and placed in a metal sample holder, with approximately 10 mm in diameter and 2.3 mm thick. The analyses were performed using a diffuse reflectance accessory (DRIFT). All experiments were carried out at room temperature.

The decomposition and the removal of the templates from the solids were monitored by differential thermal analysis (DTA) and thermogravimetry (TG). These experiments were carried out in a Mettler Toledo TGA/SDTA 851e equipment, using 5 mg of the sample which was placed in a specimen holder of alumina and heated (10 °C min^{-1}) from room temperature up to 1000 °C under air flow (50 mL min^{-1}).

The textural properties of the catalysts were determined by nitrogen adsorption and desorption experiments performed at 77 K in a Micromeritics ASAP 2020 apparatus. Before analysis, around 0.15 g of the sample were heated (10 °C min^{-1}) up to 200 °C for 2 h under vacuum and then submitted to a pressure increase up to 50 μmHg for the removal of water from the sample. During analysis, the sample was exposed to pulses of nitrogen until a maximum increase of pressure of 925 mmHg.

The transmission electron microscopy (TEM) and electron diffraction (ED) analyses were performed in a Jeol JEM 1200 EXII equipment. The samples were dispersed in ethanol and one drop of the suspension was placed on carbon-coated copper grids (150 mesh). For the electron diffraction experiments, an accelerating voltage and a focal length of 120 kV and 60 cm were used, respectively. Aluminum was used as standard for calibration.

The acidity of the solids was measured by temperature programmed desorption (TPD) using ammonia. The experiments were performed in a Micromeritics TPD/TPR 2900 equipment, on samples previously calcined

at 550 °C, for 635 min. Before analysis, the sample (0.3 g) was heated (110 ºC) under air flow (50 mL min^{-1}) for 30 min. At this temperature, pulses of ammonia were injected until saturation. The sample was then cooled to room temperature and heated up to 800 ºC to promote ammonia desorption.

Results and Discussion

Effect of aging temperature of seed gel on the properties of beta zeolite/MCM-41 materials

Figure 1 shows the X-ray diffractograms at small (Figure 1a) and high (Figure 1b) angles for the samples obtained by aging the seed gel at different temperatures (60, 90 and 140 ºC). From Figure 1a, it can be noted that a lamellar mesophase[9] or a disorganized hexagonal mesophase[38] was produced when the seed gel was aged at 60 ºC. This phase is characterized by a single peak between 2.0 and 3.0º 2θ, assigned to the reflection of the 100 plane of these materials. When the seed gel was hydrothermally treated at 140 °C, the lamellar phase was completely converted into a hexagonal mesophase. The XRD pattern of this sample showed four peaks at 1.84, 3.18, 3.66 and 4.88º assigned to the 100, 110, 200 and 210 reflections of the hexagonal structure of MCM-41, respectively.[9] At high angles (Figure 1b), by increasing the temperature of the seed aging the crystalline domains increase, the patterns being related to beta zeolite.[39]

These findings were confirmed by the infrared spectra, shown in Figure 2. A broad band between 500 and 600 cm^{-1} was noted for the B60/24 and B90/24 samples, indicating the presence of five-membered double rings, typical of beta zeolite and assigned to vibrations of the T–O–T (T = Si, Al) siloxane bonds in the rings.[40] Generally, the spectrum of the conventional beta zeolite shows two bands in this range, only one band being related to zeolitic crystals in the nanometer scale.[41] As the aging temperature increases (B140/24 sample), two bands can be observed in the range of 500-600 cm^{-1}, confirming the formation of more crystalline zeolitic precursors and/or bigger crystals as observed in the X-ray diffractograms at high angles (Figure 1b).

These results show that different mesoporous phases are formed by an intraparticle transformation during the mesostructuration step.[42] A possible explanation for the influence of the aging temperature on this step might be the different solubility and polymerization degree of silica at different temperatures. The sample prepared from the gel aged at 60 ºC might still contain unreacted amorphous silica. Therefore, the liquid phase of the aged gel contains

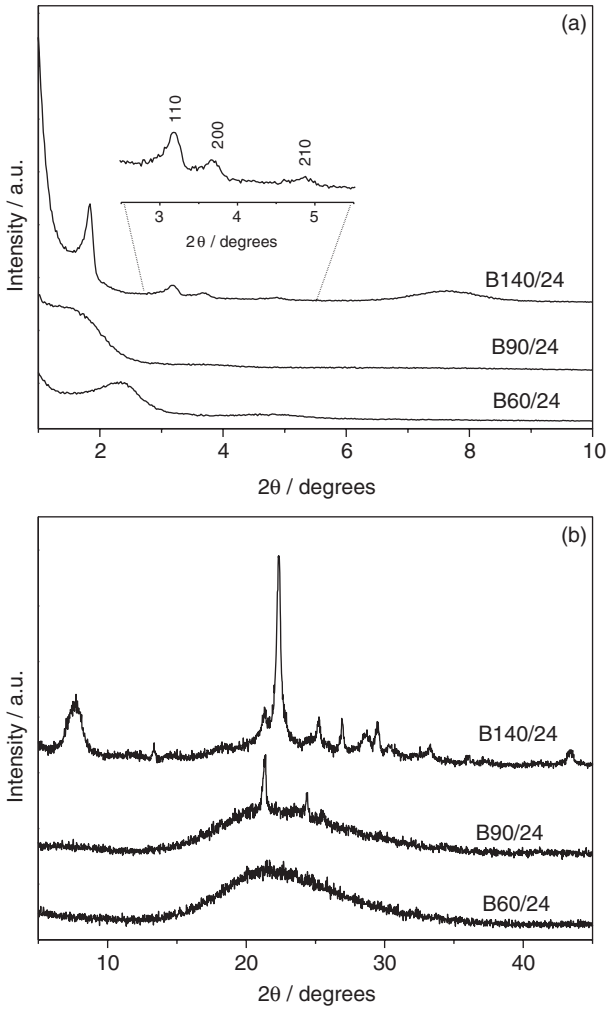

Figure 1. X-ray diffractograms of samples obtained by aging the seed gel of beta zeolite at different temperatures (60, 90 and 140 ºC) for 24 h, in the region of (a) small and (b) high angles.

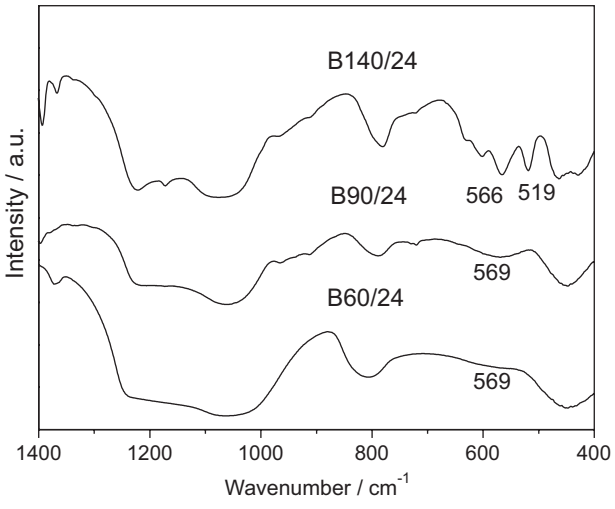

Figure 2. FTIR spectra of samples obtained by aging the seed gel of beta zeolite at different temperatures (60, 90 and 140 ºC) for 24 h; enlargement from 400 to 1400 cm^{-1}.

higher amount of less polymerized silicate than that aged at 140 ºC. The presence of less polymerized silicate (which has higher negative charge density) favors the formation of a lamellar structure, since larger amounts of positive charges are required to compensate for the negative charges. The surfactant molecules (positively charged species) then produces the lamellar arrangement with the highest positive charge density. At higher temperatures silica condensation increases and consequently a mesoporous hexagonal phase (140 ºC) is obtained.

Based on these results, it was concluded that 140 °C is the most suitable temperature to obtain a seed gel that, by mesostructuration/crystallization, led to the production of a solid containing a beta zeolite microporous phase and a hexagonally ordered mesoporous phase. Thus, in the study on the influence of time of the gel aging on the properties of the final solid, the temperature was kept constant at 140 °C.

Effect of aging time of seed gel on the properties of beta zeolite/MCM-41 materials

The structure of the solids after calcination was detected by X-ray diffraction, as shown in Figure 3a, in which the Bragg reflections of beta zeolite at high angles can be observed (101, 004, 300, 302, 304, 008 and 306 planes).[39] Table 1 shows the crystallinity of the zeolite phase, calculated from the relative intensity of the main peak (2θ = 22.4°), which is typical of a microporous structure. The B140/192 sample was used as standard.

As we can see, there is a slight increase of the crystallinity of beta zeolite with increasing aging time. Table 1 also shows that there is a slight increase of the crystal size (calculated by the Scherrer equation) of beta zeolite with increasing aging time. At small angles (Figure 3b), the pattern of the B140/24 sample showed three well-defined peaks corresponding to (100), (110) and (200) planes, which are characteristic of the hexagonal phase of mesoporous MCM-41.[9] By increasing the aging time, the peak for the (100) plane becomes wider and less intense. Also, the peaks related to the (110) and (200) planes are hardly observable, indicating that longer times lead to the formation of less ordered hexagonal mesoporous structures. In addition, a shift of the main diffraction peak of hexagonal mesoporous structure, indexed as (100), to larger angles with the increase of the aging time can also be observed. These results can be related to the increase in seed size with aging time, making the organization of the seeds around the CTAB micelles more difficult during mesostructuration. As a consequence, a less ordered mesoporous structure is thus generated, which is further hampered by the crystal growth during the crystallization step. This decrease in the ordering

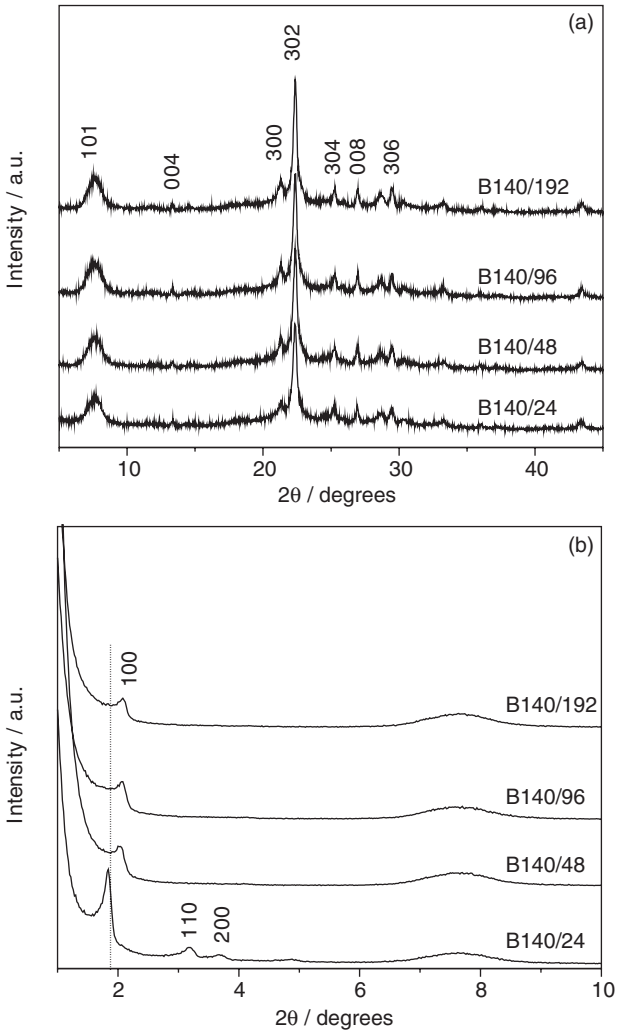

Figure 3. X-ray diffractograms for calcined samples obtained at different times (24, 48, 96 and 192 h) of seed gel aging at 140 ºC, in the region of (a) high angles and (b) small angles.

Table 1. Degree of mesoporous ordering (Goc) and crystallinity (C_{XRD}) and crystal size of the beta zeolite phase (τ) for samples after calcination (B) and after ion exchange (HB) obtained at different aging times (24, 48, 96 and 192 h) of the seed gel at 140 ºC

Samples	Goc / %	C_{XRD} / %	τ / nm
B140/24	100	79	25
B140/48	43	91	25
B140/96	41	93	27
B140/192	32	100	28
HB140/24	50	77	21
HB140/48	50	86	23
HB140/96	32	93	25
HB140/192	32	98	26

can be best detected by the degree of mesoporous ordering shown in Table 1, which was calculated using the relative intensity of the main diffraction peak of the mesoporous structure as compared to the B140/24 sample (standard).

Table 1 also shows the mesoporous ordering as well as the crystallinity and crystal size of beta zeolite in the acidic form. One can observe that the microporous crystalline structure was not significantly affected by the substitution of alkali cations by H^+ ions through ion exchange with NH_4^+. On the other hand, there was a loss of mesoporous ordering. This suggests that during the formation of MCM-41 the incorporation of aluminum occurs, resulting in the Al-MCM-41 structure (with sodium ions as compensation cations). It is known that ion exchange of sodium ions with ammonium ions and subsequent calcination results in a material in protonic form, which has lower thermal stability, in agreement with a previous work.[43]

The TG curves of the materials based on the precursors of as-synthesized beta zeolite are shown in Figure 4a. In agreement with Kleitz *et al.*,[44] these curves displayed four main stages of weight loss. The first one, at temperatures below 100 °C, is related to the desorption of water while the second and third steps, between 150 and 500 °C, are due to the decomposition and combustion of templates in beta zeolite (TEAOH) and in MCM-41 (CTAB) structures. The weight loss at higher temperatures (near 600 °C) is assigned to dehydroxylation of silanol groups and to combustion of residual coke.[44]

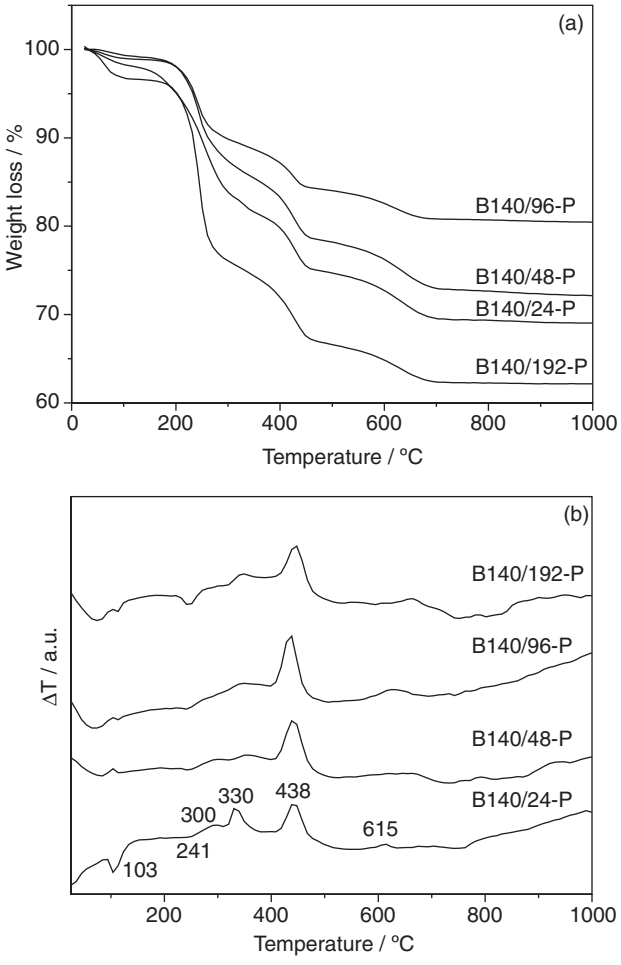

Figure 4. Curves of (a) thermogravimetry and (b) differential thermal analysis for the as-synthesized beta zeolite/MCM-41 materials (P) obtained at different aging times (24, 48, 96 and 192 h) of the seed gel at 140 ºC.

It can be noted that the weight loss changes with the aging time of the seeds (Figure 4a). In general, the longer the aging time the smaller the weight loss, except for the B140/192-P sample (Table 2). This can be assigned to the increased strength of interaction between the TEA^+ cations (template of beta zeolite) and the aluminosilicate species as a function of aging time.[45] As the aging time increases, greater condensation of the aluminosilicate species occurs, generating solids even more crystalline and/or made up of bigger crystals, as shown in Figure 3 and Table 1. However, the condensation also decreases the surface charge density and consequently the interactions of aluminosilicate species with CTA^+ species (template of MCM-41 structure). Thus, CTA^+ species which are not interacting are easily removed during washing of the solid. Therefore, these samples have lower amounts of CTAB and then showed smaller weight loss as the aging time was longer. Because of this, as aging time gets longer, the less organized the solids become. On the other hand, if this time is long enough (B140/192 sample) the crystals grow and become able to encapsulate the CTA^+ species during the crystallization step. Therefore, the CTA^+ species are not easily removed during washing and more weight was lost during the TG experiments.

Table 2. Total weight loss for the as-synthesized beta zeolite/MCM-41 materials obtained at different aging times (24, 48, 96 and 192 h) of the seed gel at 140 ºC

Samples	Weight loss / %
B140/24-P	31
B140/48-P	28
B140/96-P	20
B140/192-P	38

The differential thermal analysis (Figure 4b) shows that the template decomposition involves three steps, in accordance with previous work.[44] An endothermic peak near 250 °C can be observed, related to the elimination of trimethylamine by Hofmann degradation, leading to hydrocarbon formation. In the range from 250 to 350 °C, they go into fragmentation to produce lower molecular weight compounds. At this stage, two exothermic events can be noted, each one associated with the fragmentation of the hydrocarbon chain of the different templates. Finally, most of the oxidation processes occur between 350 to 450 °C, transforming the low molecular weight organic

compounds into carbon dioxide, water and carbonaceous residues (exothermic process).

The presence of micro and mesopores in the samples was detected by nitrogen adsorption and desorption experiments, which produced isotherms with profiles intermediate between types I and IV (Figure 5), typical of solids with micropores and mesopores.[46] The isotherm of the B140/24 sample showed two kinds of hysteresis loop in the relative pressure range (P/P_0) from 0.2 to 0.5 and higher than 0.8. The first one is characteristic of capillary condensation in a confined mesoporous structure, while the second type is associated with the presence of secondary mesopores from the interparticular spacings.[47] This sample presented a narrow pore size distribution (Figure 6), determined by the Barrett-Joyner-Halenda (BJH) method from the adsorption branch of the nitrogen isotherms[48] showing a mean diameter around 3.5 nm (Figure 6) The isotherms of the samples prepared with longer aging time showed only a large hysteresis loop between 0.5 and 1.0, confirming the disordering of the hexagonal mesoporous structure of the MCM-41, as detected by X-ray diffraction. These samples also showed a narrow pore size distribution (Figure 6) but with a smaller diameter (2.6 nm). This suggests that the organization of the zeolitic precursors somehow causes the contraction of the aluminosilicate system shaped by the surfactant.[49] In addition to the peak at 2.6 nm, a shoulder between 3.0 and 4.0 nm was observed, showing the presence of secondary mesopores.

The solids showed high specific surface areas, as displayed in Table 3. As expected, the highest value was observed for the B140/24 sample, which had the most ordered mesoporous structure. As a whole, the values of area and pore volume did not vary significantly for the other samples. Also, the samples exhibited a typical micropore volume of beta zeolite.

From the acidity measurements by ammonia desorption, the acidic strength can be classified as weak, moderate and strong, according to the desorption temperature.[50] Weak or moderate acid sites may be present in both zeolites or mesoporous aluminosilicates but strong acid sites are only

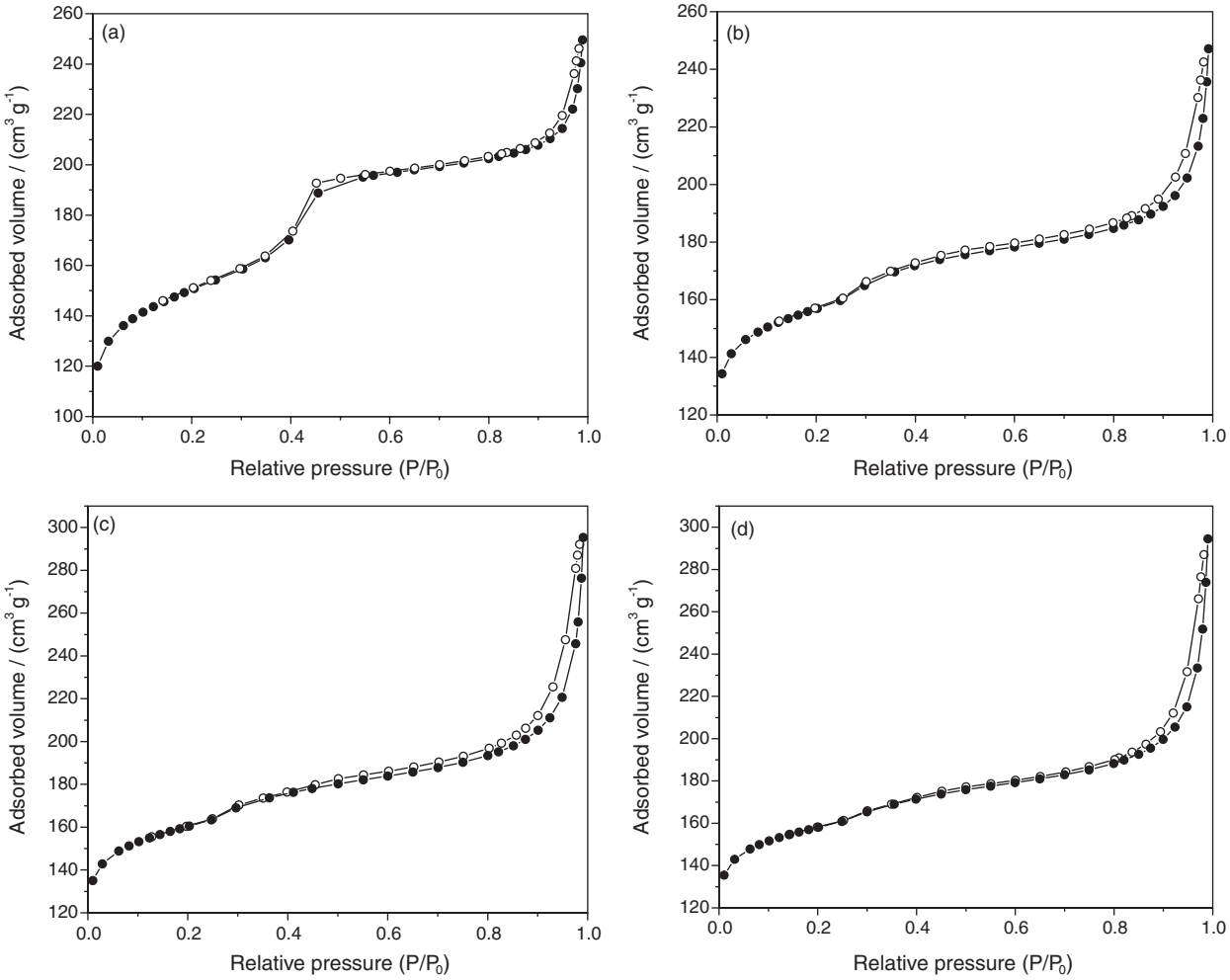

Figure 5. Nitrogen adsorption (-●-) and desorption (-○-) isotherms for the acidic form (H) of the mesostructured beta zeolite obtained at different aging times (24, 48, 96 and 192 h) of the seed gel at 140 ºC. (a) HB140/24; (b) HB140/48; (c) HB140/96 and (d) HB140/192.

Table 3. Specific surface area (Sg), external area (S_{ext}), mesopore diameter (dp), mesopore volume (V_{mp}) and micropore volume (V_m) of the beta zeolite/MCM-41 materials after calcination (B) and after ion exchange (HB) obtained at different aging times (24, 48, 96 and 192 h) of the seed gel at 140 ºC

Sample	Sg, BET / (m^2 g^{-1})	S_{ext}, *t*-plot / (m^2 g^{-1})	dp / nm	V_{mp}, BJH / (cm^3 g^{-1})	V_m, *t*-plot / (cm^3 g^{-1})
B140/24	576	270	3.5	0.27	0.16
B140/48	507	169	2.6	0.14	0.17
B140/96	509	169	2.6	0.19	0.17
B140/192	505	171	2.6	0.18	0.17
HB140/24	478	223	3.5	0.23	0.14
HB140/48	505	163	2.6	0.16	0.17
HB140/96	509	170	2.6	0.20	0.17
HB140/192	496	162	2.6	0.22	0.17

BET: Brunauer-Emmett-Teller.

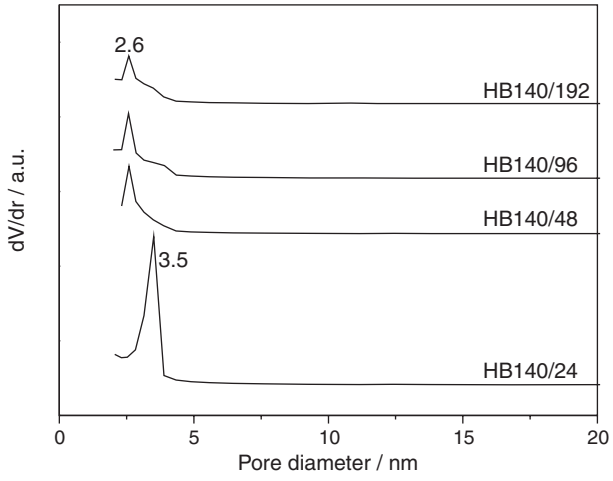

Figure 6. Pore size distribution for the acidic form (H) of beta zeolite/MCM-41 materials obtained at different aging times (24, 48, 96 and 192 h) of the seed gel at 140 ºC.

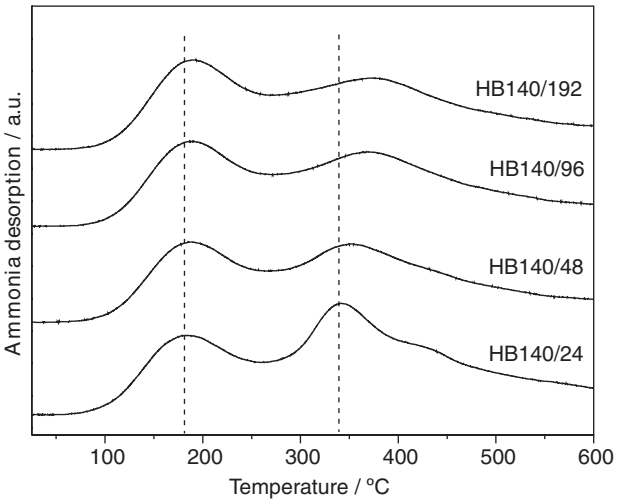

Figure 7. Number of moles of ammonia desorbed *per* gram of solid as a function of temperature, for beta zeolite/MCM-41 materials obtained at different aging times (24, 48, 96 and 192 h) of the seed gel at 140 ºC.

common in zeolites.[50-52] Figure 7 shows the curves of acidity for the samples in the acidic form, expressed as the number of moles of ammonia desorbed as a function of temperature. A low-temperature peak at 210 ºC for weak acidic sites and a high-temperature shoulder peak at 350 °C for moderate acidic sites can be found for all cases noted, in agreement with a previous work.[26]

Moreover, all samples have desorbed ammonia at temperatures above 400 °C, as shown by a shoulder (best viewed for the HB140/24 sample), related to stronger acid sites in beta zeolite. By increasing the aging time of the seeds, the maximum of the peaks of weak and moderate acid sites was shifted to higher temperatures, indicating that solids with stronger weak and moderate acid sites were produced.

Table 4 shows the results of acidity measurements for zeolites in the protonic form expressed as the number of moles of desorbed ammonia molecules *per* gram of solid as a function of temperature. It can be seen that the materials showed similar acidities, a fact that is consistent with the same silica to alumina ratios (SAR) of the seed gel for all samples. The highest acidity shown by the HB140/24 sample can be related to the highest external area of this material, which consequently provides a greater number of more easily accessible acid sites.[47] It can be observed that the HB140/192 sample showed the highest amount of acid sites *per* external area, as shown in Table 4.

Figure 8 displays the images obtained by transmission electron microscopy, which show particles with irregular shape and heterogeneous characteristics, indicating that the solids are made up of more than one phase (Figure 8a). From Figure 8b one can see very well-defined hexagonal mesoporous structure (marked as "meso") associated with beta zeolite/MCM-41 materials. Similar results were obtained by Bagshaw *et al.*.[32] On the other hand, crystalline domains were also detected as shown by the electron diffraction image (Figure 8c), in which we can see discrete diffraction spots related to (101), (004), (302) and (008) planes,[39] which are typical of the BEA structure.

Table 4. Number of moles of ammonia desorbed *per* gram of solid as a function of temperature for beta zeolite/MCM-41 materials obtained at different aging times (24, 48, 96 and 192 h) of the seed gel at 140 ºC

Sample	Acid sites / (mmol of NH_3 g^{-1} of the solid)				Acid sites *per* S_{ext} / (mmol of NH_3 m^{-2})
	Weak (T < 250 ºC)	Moderate (250 < T < 350 ºC)	Strong (T > 400 ºC)	Total	
HB140/24	0.46 (28%)	0.72 (42%)	0.53 (30%)	1.71	0.0076
HB140/48	0.38 (30%)	0.69 (54%)	0.20 (15%)	1.27	0.0078
HB140/96	0.40 (31%)	0.79 (61%)	0.11 (8%)	1.30	0.0076
HB140/192	0.44 (32%)	0.83 (60%)	0.11 (8%)	1.38	0.0085

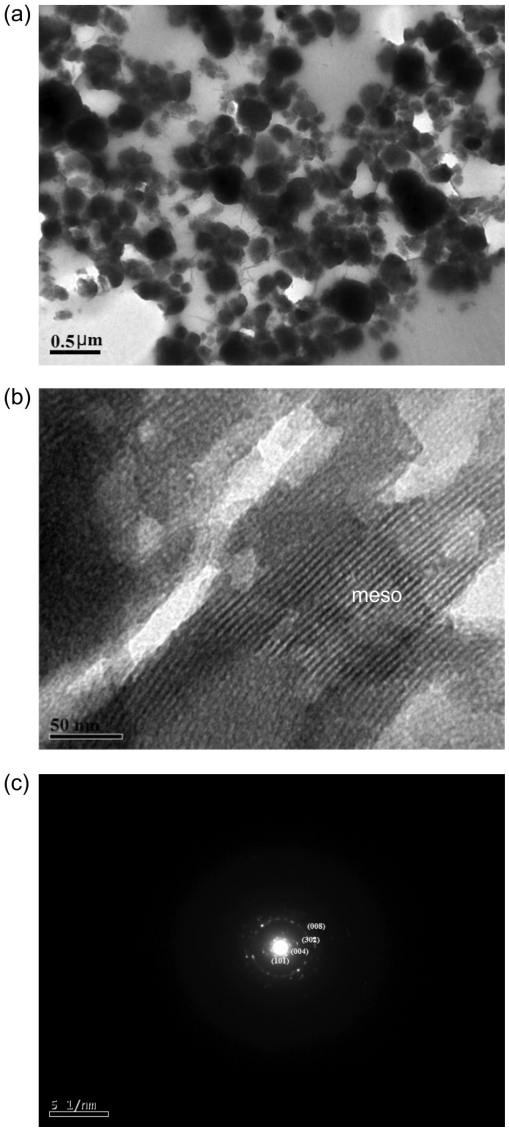

Figure 8. (a) TEM image of HB140/192 sample; (b) TEM image of HB140/96 sample showing the mesophase domain and (c) electron diffractogram showing the domain corresponding to the crystalline phase.

These results indicate that the samples are made up of two phases: (*i*) a crystalline one corresponding to the high stable beta zeolite, which is unchanged after synthesis and post-treatment and (*ii*) a mesoporous MCM-41 with low thermal and hydrothermal stability. Therefore, a mesoporous phase was formed by an intraparticle transformation during the mesostructuration step but not all seeds were converted to the mesoporous phase and a beta zeolite phase is formed independently.

Conclusions

The aging temperature of the seed gel of beta zeolite influences the mesophase type that is formed during the mesostructuration step. Only at high aging temperature (140 °C) a mesoporous hexagonal phase of MCM-41 is obtained. This sample consists of a crystalline microporous phase of beta zeolite responsible for strong acid sites in the solid and a mesoporous phase corresponding to MCM-41, which provided high specific surface area and is responsible for the weak and moderate acid sites in the solid. Increasing the aging time from 24 to 192 h, at 140 °C, decreases the crystallinity and favors the growth of zeolite seeds which form bigger crystals that hardly fit into the mesoporous wall. Moreover, the strength of weak and moderate acid sites tends to increase as a function of aging time. The size and the crystallinity of the zeolite and the ordering of mesoporous phases in the materials can be tailored by the time of seed aging and then the described synthesis may allow the preparation of tailored-made catalysts for the transformation of bulky molecules.

Supplementary Information

Supplementary data are available free of charge at http://jbcs.sbq.org.br as PDF file.

Acknowledgements

S. T. F. G. acknowledges CNPq for his scholarship. This work was supported by CNPq and FINEP. This work is dedicated to the memory of our colleague and friend, Prof. Roberto Fernando de Souza, who prematurely left us.

References

1. Bellussi, G.; Carati, A.; Millini, R. In *Zeolites and Catalysis. Synthesis, Reactions and Applications*; Cejka, J.; Corma, A.; Zones, S., eds.; Wiley-VCH: Weinheim, 2010, pp. 449.
2. Mahmoud, E.; Lobo, R. F.; *Microporous Mesoporous Mater.* **2014**, *189*, 97.
3. Ramos, M. S.; Grecco, S. T.; Gomes, L. P.; Oliveira, A. C.; Reyes, P.; Oportus, M.; Rangel, M. C.; *Stud. Surf. Sci. Catal.* **2005**, *156*, 809.
4. Rangel, M. C.; Grecco, S. T. F.; Carvalho, D. R.; Urquieta-González, E. A.; Grau, J. M.; Reyes, P.; Oportus, M. In *Xylenes: Synthesis, Characterization and Physicochemical Properties*; Daramola, M. O., ed.; Nova Science Publishers: New York, 2013, pp. 57.
5. Fonseca, J. D. S. L.; Júnior, A. D. C. F.; Grau, J. M.; Rangel, M. C.; *Appl. Catal., A* **2010**, *386*, 201.
6. Corma, A.; *Chem. Rev.* **1997**, *97*, 2373.
7. Corma, A.; *Chem. Rev.* **1995**, *95*, 559.
8. Domingues, S. M.; Britto, J. M.; Oliveira, A. S.; Valentini, A.; Reyes, P.; David, J. M.; Rangel, M. C.; *Stud. Surf. Sci. Catal.* **2001**, *139*, 45.
9. Beck, J. S.; Vartuli, J. C.; Roth, W. J.; Leonowicz, M. E.; Kresge, C. T.; Schmitt, K. D.; Chu, C. T.-W.; Olson, D. H.; Sheppard, E. W.; McCullen, S. B.; Higgins, J. B.; Schlenker, J. L.; *J. Am. Chem. Soc.* **1992**, *114*, 10834.
10. Tanev, P. T.; Pinnavaia, T. J.; *Science* **1995**, *267*, 865.
11. Zhao, D.; Feng, J.; Huo, Q.; Melosh, N.; Fredrickson, G. H.; Chmelka, B. F.; Stucky, G. D.; *Science* **1998**, *279*, 548.
12. Trong On, D.; Desplantier-Giscard, D.; Danumah, C.; Kaliaguine, S.; *Appl. Catal., A* **2003**, *253*, 545.
13. van Donk, S.; Janssen, A. H.; Bitter, J. H.; de Jong, K. P.; *Catal. Rev.* **2003**, *45*, 297.
14. Hartmann, M.; *Angew. Chem., Int. Ed.* **2004**, *435*, 880.
15. Pérez-Pariente, J.; Díaz, I.; Agúndez, J.; *C. R. Chim.* **2005**, *8*, 569.
16. Egeblad, K.; Christensen, C. H.; Kustova, M.; Christensen, C. H.; *Chem. Mater.* **2008**, *20*, 946.
17. Grecco, S. T. F.; Rangel, M. C.; Urquieta-Gonzalez, E. A.; *Quim. Nova* **2013**, *36*, 131.
18. Liu, Y.; Zhang, W.; Pinnavaia, T. J.; *J. Am. Chem. Soc.* **2000**, *122*, 8791.
19. Prokešová, P.; Žilková, N.; Mintova, S.; Bein, T.; Čejka, J. C.; *Appl. Catal. A* **2005**, *281*, 85.
20. Liu, Y.; Zhang, W.; Pinnavaia, T. J.; *Angew. Chem., Int. Ed.* **2001**, *40*, 1255.
21. Guo, W.; Huang, L.; Deng, P.; Xue, Z.; Li, Q.; *Microporous Mesoporous Mater.* **2001**, *44-45*, 427.
22. Shih, P.-C.; Wang, J.-H.; Mou, C.-Y.; *Catal. Today* **2004**, *93-95*, 365.
23. Gonçalves, M. L.; Dimitrov, L. D.; Wallau, M.; Urquieta-Gonzalez, E. A.; *Stud. Surf. Sci. Catal.* **2006**, *162*, 323.
24. Wang, S.; Dou, T.; Li, Y.; Zhang, Y.; Li, X.; Yan, Z.; *J. Solid State Chem.* **2004**, *177*, 4800.
25. Liu, Y.; Pinnavaia, T. J.; *Chem. Mater.* **2002**, *14*, 3.
26. Guo, W.; Xiong, C.; Huang, L.; Li, Q.; *J. Mater. Chem.* **2001**, *11*, 1886.
27. Zhang, Z.; Han, Y.; Xiao, F.-S.; Qiu, S.; Zhu, L.; Wang, R.; Yu, Y.; Zhang, Z.; Zou, B.; Wang, Y.; Sun, H.; Zhao, D.; Wei, Y.; *J. Am. Chem. Soc.* **2001**, *123*, 5014.
28. Zebib, B.; Zeng, S.; Krafft, J.-M.; Lambert, J.-F.; Blanchard, J.; Nie, H.; Li, D.; Breysse, M.; *Stud. Surf. Sci. Catal.* **2005**, *158*, 517.
29. Petushkov, A.; Merilis, G.; Larsen, S. C.; *Microporous Mesoporous Mater.* **2011**, *143*, 97.
30. Ooi, Y.-S.; Zakaria, R.; Mohamed, A. M.; Bhatia, S.; *Appl. Catal., A* **2004**, *274*, 15.
31. García, R. A.; Serrano, D. P.; Otero, D.; *J. Anal. Appl. Pyrolysis* **2005**, *74*, 379.
32. Bagshaw, S. A.; Baxter, N. I.; Brew, D. R. M.; Hosie, C. F.; Yuntong, N.; Jaenicke, S.; Khuan, C. G.; *J. Mater. Chem.* **2006**, *16*, 2235.
33. Bordoloi, A.; Devassy, B. M.; Niphadkar, P. S.; Joshi, P. N.; Halligudi, S. B.; *J. Mol. Catal. A: Chem.* **2006**, *253*, 239.
34. Odedairo, T.; Balasamy, R. J.; Al-Khattaf, S.; *J. Mol. Catal. A: Chem.* **2011**, *345*, 21.
35. Pereira, A. L. C.; González-Carballo, J. M.; Pérez-Alonso, F. J.; Rojas, S.; Fierro, J. L. G.; Rangel, M. C.; *Top. Catal.* **2011**, *54*, 179.
36. Bejblová, M.; Žilková, N.; Čejka, J.; *Res. Chem. Intermed.* **2008**, *34*, 439.
37. Jansen, J. C.; Creyghton, E. J.; Njo, S. L.; van Koningsveld, H.; van Bekkum, H.; *Catal. Today* **1997**, *38*, 205.
38. Chen, C.-Y.; Xiao, S.-Q.; Davis, M. E.; *Microporous Mater.* **1995**, *4*, 1.
39. Treacy, M. M. J.; Higgins, J. B.; *Collection of Simulated XRD Powder Patterns for Zeolites*, 5th ed.; Elsevier Science: Amsterdam, 2007.
40. Flanigen, E. M. In *Zeolite Chemistry and Catalysis*; Rabo, J. A., ed.; American Chemical Society: Washington, 1976, pp. 80.
41. Prokešová, P.; Mintova, S.; Čejka, J.; Bein, T.; *Mater. Sci. Eng., C* **2003**, *23*, 1001.
42. Gonçalves, M. L.; Dimitrov, L. D.; Jordão, M. H.; Wallau, M.; Urquieta-González, E. A.; *Catal. Today* **2008**, *133-135*, 69.
43. Kim, J. M.; Kwak, J. H.; Jun, S.; Ryoo, R.; *J. Phys. Chem.* **1995**, *99*, 16742.
44. Kleitz, F.; Schimidt, W.; Schüth, F.; *Microporous Mesoporous Mater.* **2003**, *65*, 1.
45. Huang, L.; Guo, W.; Deng, P.; Xue, Z.; Li, Q.; *J. Phys. Chem. B* **2000**, *104*, 2817.
46. Schneider, P.; *Appl. Catal., A* **1995**, *129*, 157.
47. Camblor, M. A.; Corma, A.; Valencia, S.; *Microporous Mesoporous Mater.* **1998**, *25*, 59.

48. Barrett, E. P.; Joyner, L. G.; Halenda, P. P.; *J. Am. Chem. Soc.* **1951**, *73*, 373.
49. Bagshaw, S. A.; Jaenicke, S.; Khuan, C. G.; *Catal. Commun.* **2003**, *4*, 140.
50. Tang, T.; Yin, C.; Wang, L.; Ji, Y.; Xiao, F.-S.; *J. Catal.* **2008**, *257*, 125.
51. Wang, J.; Huang, L.; Chen, H.; Li, Q.; *Catal. Lett.* **1998**, *55*, 157.
52. Grecco, S. T. F.; Gomes, L. P.; Reyes, P.; Oportus, M.; Rangel, M. C.; *Stud. Surf. Sci. Catal.* **2005**, *158*, 1937.

Submitted: August 13, 2014
Published online: November 18, 2014

FAPESP has sponsored the publication of this article.